

Axial phase of quantum fluids in nanotubes

S. M. Gatica^{1,2}, G. Stan^{2,3}, M. M. Calbi¹, J. K. Johnson⁴ and M. W. Cole^{2,5}

¹*Departamento de Física, Universidad de Buenos Aires, Buenos Aires 1428, Argentina.*

²*Department of Physics and Center for Materials Physics,*

Pennsylvania State University, University Park, PA 16802, USA.

³*Present address: Institute for Physical Science and Technology and*

Department of Chemical Engineering, University of Maryland, College Park, MD 20742, USA.

⁴*Department of Chemical and Petroleum Engineering,*

University of Pittsburgh, Pittsburgh, PA, 15260, USA.

⁵*corresponding author, e-mail: mwc@psu.edu, phone: 814-863-0165, fax: 814-865-3604*

(March 9, 2019)

Abstract

We explore the equations of state and other properties of various quantum fluids (³He, ⁴He, their mixtures, and H₂) confined within individual carbon nanotubes. Above a threshold number of particles, N_a , the fluid density near the axis begins to grow above a negligibly small value. The properties of this axial fluid phase are sensitive to the tube size and hence to the transverse compression in the case of a bundle of nanotubes. We consider He at zero temperature and H₂ at low temperatures.

I. INTRODUCTION

The physical properties of carbon nanotubes are expected to manifest a variety of intriguing one-dimensional (1d) and quasi-1d behaviors [1–13]. We, and other groups, have found that fluids absorbed within these tubes ought to exhibit an “effective” dimensionality

which is sensitive to the geometry, species, number (N) of particles and temperature (T). For example, in the case of isolated nanotubes, the ideal gas regime of very low N , is predicted to show crossover between 1d and 2d behavior as T increases, due to the excitation of azimuthal motion of the atoms adsorbed on the inner wall of the tubes [13]. For a bundle of nanotubes, in contrast, it has been predicted and found experimentally that low N gases which have small diameter are adsorbed strongly in interstitial channels, between tubes, in which the gases display 1d motion [5,8,11,14]. Larger diameter gases adsorb preferentially within the tubes. [15,16]

The novel collective properties of the absorbed interacting fluid at higher N are now being explored. In this paper we consider the evolution, as a function of N , of the structure and properties of dense quantum fluids within individual nanotubes at $T = 0$. Consider He for specificity. Above the ideal gas regime of density, there appears a regime of density in which liquid ^4He is adsorbed on the walls of the tube; we call this a cylindrical “shell” phase [17]. At somewhat higher density this fluid should solidify; we expect that this film is similar to the much studied incommensurate monolayer solid film on graphite [18–20]. For values of N below a threshold value N_a there exists only this shell phase. We predict here a transition in which there appears, for $N > N_a$, an axial phase of this fluid, signified by the presence of a fluid confined to the vicinity of the tube axis. This axial phase transition is qualitatively similar to two other transitions familiar in the field of adsorption: capillary condensation (CC) and the layering transition [21,22]. While the latter (2d) transition is known to occur at finite T , the appearance of the axial phase is a genuine thermodynamic transition only at $T = 0$ because the geometry is 1d, so that fluctuations eliminate the transitions at higher T . This feature is also the case for a CC transition in a single pore, but often in experiments the effect of interactions with other pores is such as to permit a CC transition at nonzero T [4,5]. Similar behavior of the axial phase transition should occur in a nanotube bundle (“rope”), but we have not yet investigated that problem. Also, the same phenomenon is expected to occur for a classical system since nothing specifically related to quantum effects plays a paramount role [6,23].

We have investigated the axial phase with three distinct methods. The next section presents Hartree model calculations for four systems: ^4He , ^3He , their mixtures, and H_2 .

These calculations rely extensively on the use of other workers' calculations and data for 2d quantum systems [24–26]. Section III presents results of Path Integral Monte Carlo studies of H_2 . Section IV reports results for ^3He - ^4He mixtures, obtained with the Hartree approach. Section V describes the results obtained with Density Functional calculations applied to ^4He [27]. The comparison between our various approaches is interesting, as is that between the present data and “exact” results for ^4He in 1d [8]. Section VI summarizes our results and conclusions.

II. HARTREE MODEL CALCULATIONS FOR HELIUM AND HYDROGEN

Our goal is to determine the threshold coverage for formation of the axial phase. The general approach described in this section is analogous to that used in previous studies of the problem of layer promotion [24,28]. The assumption is made that, above threshold, atoms (or molecules in the case of H_2) form two coexisting phases, the axial phase and the shell phase. These are characterized by 1d densities N_a/L and N_s/L , respectively. The condition for equilibrium is that the chemical potentials of the two phases coincide:

$$\mu_{\text{axial}} = \mu_{\text{shell}} \quad (1)$$

The axial phase is thought of as a 1d phase affected by the “external” Hartree potential provided by the shell phase and the host nanotube. Its chemical potential is assumed to satisfy

$$\mu_{\text{axial}}(N_a/L) = \epsilon_a + \mu_{1d}(N_a/L) \quad (2)$$

The 1d approximation ought to be valid here in that we focus on the regime when the rms displacement transverse to the axis is small compared to the axial phase interparticle spacing and the axial and shell atoms are well separated spatially. Here $\mu_{1d}(N_a/L)$ is the chemical potential of a 1d fluid at density N_a/L and ϵ_a is the eigenvalue of the atoms in the Hartree potential. At the threshold for forming the axial phase, μ_{1d} assumes its lowest value, the ground state cohesive energy of the 1d fluid. This energy has been found previously for ^4He to be of order 2 mK, which is negligible small in the present context, so we ignore it for ^4He and the other cases studied here [29].

The energy ϵ_a was computed from a numerical solution of the Schrödinger equation for ground state (zero angular momentum) atomic motion in the Hartree potential:

$$V_{tot}(r) = V_C(r) + \theta V_H(r) \quad (3)$$

where $V_C(r)$ is the potential near the axis due to the carbon atoms alone computed in the assumption of smooth tube walls as in previous studies [7]. The second term is a Hartree interaction, where θ is the density of gas atoms/molecules in the shell, and $\theta V_H(r)$ is the interaction due to the shell:

$$V_H(r) = \int d\mathbf{r}' |\Psi_s(\mathbf{r}')|^2 U_{gg}(|\mathbf{r} - \mathbf{r}'|) \quad (4)$$

where $\Psi_s(\mathbf{r}')$ is the wave function of gas atoms/molecules in the shell and U_{gg} is the gas-gas interaction. We make the further approximation of assuming that the atoms in the shell phase are narrowly confined in the radial direction:

$$|\Psi_s(\mathbf{r})|^2 \sim \delta(r - R) \quad (5)$$

where R is the radius of the cylindrical surface near which the atoms are situated. Then the evaluation of V_H reduces to integrations over the longitudinal and azimuthal coordinates, as shown in Ref. [7].

The ground state eigenfunction of the Schrödinger equation for an atom close to the axis is of the form $\Psi_a(\mathbf{r}) = f(r) \exp(ikz)$, where r and z are the cylindrical coordinates of the atom's position vector \mathbf{r} . The eigenvalue ϵ_a is then determined from the differential equation satisfied by the ground state radial wave function, $f(r)$:

$$\frac{d^2 f}{dr^2} + \frac{1}{r} \frac{df}{dr} + \frac{2m}{\hbar^2} [\epsilon_a - V_{tot}(r)] f(r) = 0 \quad (6)$$

We solve this equation numerically.

Figures 1 and 2 display for the He isotopes the two chemical potentials appearing in Eq. 1; their curves' crossing occurs at the threshold at which the axial phase appears. The abscissa in these figures is a 2d density of the shell phase:

$$\theta = N_s / (2\pi RL) \quad (7)$$

As seen in figures 1 and 2, the eigenvalue ϵ_a is a nearly linear function of the shell phase density in the neighborhood of the transition, as expected from a perturbation theory of the Hartree interaction, based on Eq. 3.

We have made the simplest plausible assumption for the function $\mu_{shell}(\theta)$ - that it coincides with the 2d chemical potential on graphite, apart from an additive constant arising from the stronger substrate attraction and resulting larger binding energy in the tubes:

$$\mu_{shell}(\theta) = \mu_{graphite}(\theta) + \Delta E_b \quad (8)$$

Here ΔE_b is the difference in binding energy between the result for the nanotubes [13] and that for graphite [26,30]. The justification for this implicit neglect of the effect of curvature appears in the Appendix. Our values of these functions $\mu_{shell}(\theta)$ are taken from theoretical studies of Ref. [24,25] which are consistent with experiments reported in Ref. [26].

The key properties of the shell and axial phases at threshold are displayed in Tables I and II and Fig. 3 for the isotopes ^4He and ^3He , respectively. There are no significant differences between the qualitative behaviors of the two isotopes. Consider, for example, the case of ^4He within nanotube having a radius of $R_C = 6 \text{ \AA}$. Note that the He shell radius, $R = 3.06 \text{ \AA}$, is about 3 \AA closer to the axis than is the carbon shell; R increases by ca. 1 \AA as R_C increases by 1 \AA . As R_C increases, the energy levels of the shell (E_0) and axial states at threshold increase monotonically. The threshold density θ_c of the shell state is insensitive to this change, remaining close to the known value 0.115 \AA^{-2} for monolayer completion density on graphite [25,31]. However, the threshold chemical potential μ_c varies much more; it increases by about 20 K for each 1 \AA change in R ; for $R_C = 8 \text{ \AA}$, μ_c approaches the value -35 K for monolayer completion on graphite [32]. Note that the potential energy responsible for the axial state changes by an even larger amount than μ_c . The minimum value of the total potential energy, $V_{tot}(r_{min})$, changes by 90 K as R_C increases by 2 \AA , while μ_c changes by only 40 K. The reason is that the zero point kinetic energy also changes significantly, as can be understood from the uncertainty principle. The kinetic energy is much larger at $R_C = 6 \text{ \AA}$, for which state the root mean square radial coordinate is $r_{rms} = 0.41 \text{ \AA}$, than at $R_C = 8 \text{ \AA}$, for which $r_{rms} = 2 \text{ \AA}$. Note from the table that the carbon shell's contribution to the potential energy $V_C(r)$ is typically 40% of the total potential energy while the He

shell contribution is about 60%; these proportions change slowly as R_C changes. Finally, we note the qualitative change in the axial state wave function seen in Fig. 3. For the case of $R_C = 8 \text{ \AA}$, the axial state's probability density is no longer confined to the immediate vicinity of the axis, exhibiting a maximum near $r = 2 \text{ \AA}$. One observable property which is determined by this spread is the momentum distribution function, which ought to be much narrower in the case of such a dispersed wave function. We intend to consider this topic in future work.

Figures 4 and 5 and Table III present the results of analogous calculations for H_2 adsorption in nanotubes of varying size. The data corresponding to $R_C = 8 \text{ \AA}$ look qualitatively similar to those for He except with different numerical values, of course. As for ^4He , the threshold values of coverage and chemical potential are similar to those for monolayer completion on graphite ($\theta_c = 0.094 \text{ \AA}^{-2}$, $\mu_c = -244 \text{ K}$) [33].

For $R_C = 7 \text{ \AA}$, the axial phase threshold value of the chemical potential for H_2 , i.e. the crossover seen in Fig. 4, moves to a much lower value ($\mu_c = -385 \text{ K}$) than for $R_C = 8 \text{ \AA}$ (-261 K). For the smallest case studied, $R_C = 6 \text{ \AA}$, we find no crossing of the chemical potential curves. This means simply that nanotubes which are so small do not produce an axial phase, according to our calculations.

III. PATH INTEGRAL SIMULATIONS FOR HYDROGEN

As a check on the validity of the Hartree calculations we have performed molecular simulations of hydrogen adsorption in nanotubes, using the path integral formalism [34] implemented in the grand canonical ensemble. The algorithm we have used follows the previous work of Wang and Johnson [35,36]. The Silvera-Goldman [37] isotropic interaction potential was used for the $\text{H}_2\text{-H}_2$ potential. The nanotube-hydrogen potential used in the path integral simulations was the same as that used in the Hartree calculations. The path integral calculations were carried out at finite temperature, so we do not expect complete agreement with the Hartree method. In particular, the shell-axial first order phase change will disappear in favor of a continuous transition as the axial phase is populated. Calculations were performed at 5 and 10 K for nanotubes of radius 5, 6, 7, and 8 \AA . In the path integral

formalism each quantum molecule is replaced by a classical ring polymer containing some number of beads. The accuracy of the simulations depends on the number of beads used in each ring, with the results becoming exact as the number of beads per ring approaches infinity. We found that 50 beads per ring were sufficient to obtain convergent results at both 5 and 10 K.

The shell and axial phase densities of hydrogen in the 7 Å tube are plotted in figure 6 as a function of the chemical potential. The shell phase density remains fairly constant while the axial phase increases dramatically at a chemical potential of about -375 K, in reasonable agreement with the Hartree value of $\mu_c = -385$ K given in Table III. The results at a temperature of 5 K (not shown) are very similar, but the population of the axial phase commences at a somewhat higher chemical potential. The shell and axial phase densities for the 6 Å radius nanotube are shown in figure 7. The path integral calculations demonstrate that population of the axial phase does occur, with the onset at a chemical potential of about -325 K. This is inconsistent with the Hartree calculations, which do not show the formation of an axial phase at any chemical potential for this small value of R.

Figure 8 is a plot of the density profile in the 6 Å nanotube at three different chemical potentials. Note from figure 8 that the location of the shell phase is pushed progressively outward in response to the increased population of the axial phase. The disagreement between the Hartree and path integral calculations can be ascribed to the fact that the Hartree model does not account for the shift in the location of the shell phase due to the presence of the axial phase, and therefore the Hartree model misses the axial phase observed in the simulations. The density profile for the 7 Å tube is plotted in figure 9 for a series of chemical potentials. Note that that shell phase is essentially unperturbed by the presence of the axial phase in the 7 Å nanotube.

The coverage and density profiles for the 8 Å nanotube are plotted in figures 10 and 11, respectively. Note that the onset of axial phase population occurs at a higher chemical potential (larger bulk pressure) than for either the 6 or 7 Å nanotube. This is somewhat surprising given that the shell phase must be compressed in order to make way for the axial phase in the 6 Å tube. The onset of population of the axial phase in the 8 Å nanotube occurs at about $\mu = -298$ K, in fair agreement with the Hartree value of $\mu_c = -261$ K from

Table III. Note from figure 11 that it is evident that the 8 Å nanotube does not actually have an axial phase, but rather a second shell phase, centered about 2 Å from the center of the tube. This agrees with the Hartree calculations of figure 5.

IV. HELIUM MIXTURES

We now consider the case of isotopic mixtures of helium adsorbed at medium to high density within the tube. In the analogous situation on the graphite basal plane, there is complete isotopic separation at $T = 0$ [38]. We expect the same behavior in the nanotubes at coverages below that required for producing the axial phase. In this case, the criterion determining the distribution of the two phases on the surface is equality of their spreading pressures. Figure 12 presents the coexisting 2d densities of these phases, as derived from application of this criterion to the equation of state data of Bruch [39] and Figure 13 shows a schematic view of the mixture configuration, determined by computing the threshold for the axial phase. We found that ^3He atoms first go to the axial region surrounded by the ^4He atoms at virtually the same spreading pressure at which ^4He atoms begin to go on the axis. The preferential binding in the ^4He region is a consequence of the higher 2d shell density at ^3He - ^4He coexistence. Our numerical results for this onset condition appear in Figure 14 and Table IV.

V. DENSITY FUNCTIONAL STUDY OF ^4HE

We consider that the energy of an ensemble of N helium atoms in the nanotube has the form

$$E[\rho] = E_0[\rho] + \int d\mathbf{r} \rho(r) V_C(r) \quad (9)$$

where $V_C(r)$ is the adsorption potential due to all the carbon atoms in the nanotube evaluated at point \mathbf{r} and $E_0[\rho]$ is the Finite Range Density Functional (FRDF) that represents the energy of inhomogeneous ^4He . The form of $E_0[\rho]$ and the discussion of formalism can be found in Ref. [27]. Such density functionals have previously been applied to the study of adsorbed films [40] and impurity atoms in liquid He. [41]

At zero temperature, the density of the N helium atoms is $\rho(r) = N|\Psi(r)|^2$, where $\Psi(r)$ is the single particle ground state wave function that minimizes the energy $E[\rho]$. The minimization procedure leads to the following Hartree-Fock equation for Ψ ,

$$(-(\hbar^2/2m) \nabla^2 + U[\rho]) \Psi = \mu \Psi \quad (10)$$

Here $U[\rho]$ is the effective single particle interaction and is equal to

$$U[\rho] = \delta E / \delta \rho. \quad (11)$$

The ground state wave function, Ψ , depends only on the distance to the axis of the nanotube, r , and equation 10 becomes one-dimensional. We compute Ψ and μ by solving equation 10 self-consistently. The results are displayed in figures 15-17, for the 6 Å nanotube.

In figure 15 we plot the density as a function of the radial coordinate r for different values of the chemical potential. For small μ the density has only one peak centered at $R = 3.06$ Å. As long as the value of μ increases, the height of this peak grows, reaching densities much larger than the saturation density of bulk ${}^4\text{He}$ (0.022 Å $^{-3}$), suggesting the formation of a solid phase (which is not accurately described by our method). For larger μ the axial peak becomes appreciable and continues to grow as μ increases, while the shell peak remains constant. The picture agrees very well with the model we proposed in section II.

We evaluated the number of atoms in the axial region, N_a , and in the shell region, N_s , by integrating each of the peaks of the density. In figure 16 we plot the axial density N_a/L and the shell density $\theta = N_s/(L2\pi R)$ vs. μ . As we can see N_a/L is non-zero for μ greater than $\mu_c = -108$ K. This axial phase threshold corresponds to $N/L=2.2$ Å $^{-1}$ and to $\theta_c=0.113$ Å $^{-2}$ in agreement with our previous Hartree model's prediction (see table I).

The energy per atom and the chemical potential μ are displayed in figure 17. Note a kink in the μ curve at the axial phase threshold. This effect can be attributed to the presence of a “gas-like” axial phase, since $d\mu/dN$ is proportional to the inverse of the compressibility.

VI. CONCLUSIONS

In this work we have presented various calculations pertaining to a hypothetical quasi-one-dimensional axial phase of quantum fluids adsorbed in nanotubes. Such a phase ought to be thermodynamically distinct from the high density cylindrical shell phase at lower density. Our calculations use an approximate Hartree model for H_2 and the He isotopes. Low temperature path integral calculations for H_2 are qualitatively consistent with the Hartree results, apart from the case of very small R . For 4He , a density functional model yields results which are also consistent with those of the Hartree method. We find such an axial phase in all of these cases, except for very small tubes containing H_2 . We note that similar behavior is expected for classical fluids consisting of small atoms, e.g. Ne and Ar. [6] Both our methodology and the results presented here are qualitatively similar to those obtained previously for the problem of determining the monolayer completion of quantum gases adsorbed on graphite [24,28]. Quantitatively, however, there is a big difference: the threshold chemical potential values are lower for small tubes than for a flat surface, due to the higher effective coordination of the particles in small tubes.

We have not addressed here one of the most important questions: what are the properties of this axial phase? We expect these to be entirely different from those of the second layer on graphite because of the difference in dimensionality. In particular, we anticipate the behavior to be that of the so-called “Luttinger liquid” in one dimension. Among the most remarkable of these properties for fermions are the absence of a fermi surface and the dominant role of spin and density fluctuations at low T . We hope that relevant calculations and experiments are soon forthcoming.

ACKNOWLEDGMENTS

We are grateful to M. J. Bojan, M. Boninsegni, M. W. H. Chan, V. H. Crespi, P. C. Eklund, R. B. Hallock, S. Hernandez, W. A. Steele and K. Williams for helpful discussions. This research has been supported by ARO, NSF, the University of Buenos Aires, and the Petroleum Research Fund of the American Chemical Society.

APPENDIX Curvature correction to energy

We here compute the leading curvature correction to the potential energy $P(R)$ per atom located on a cylindrical surface of infinite length and radius R . It is typical in such cases to find an expansion of the form:

$$\frac{P(R)}{P(\infty)} \sim 1 + \left(\frac{b}{R}\right)^2 \quad (12)$$

where b is a characteristic length of the system, assumed to be small compared to R in the present asymptotic limit. We shall confirm this expectation here.

It is reasonable to identify the curvature correction as arising primarily from the attractive part of the interatomic interaction since that experiences a larger distance scale than the repulsive part of the interaction and so becomes comparable to R first as the graphene sheet is curved. The attraction varies as

$$V(r) \sim -\frac{C}{r^6} \quad (13)$$

where C is the interatomic dispersion coefficient. For the case of atoms having 2d density θ ,

$$-2\frac{P(R)}{C\theta} = R \int dz \int d\varphi \frac{1}{[z^2 + (2R\sin(\varphi/2))^2]^3}. \quad (14)$$

where the 2 on the left side avoids double-counting and we bear in mind that eventually we will need a small distance cutoff ($r = a$) in order to get a finite answer. The planar limit, $R = \infty$, involves only small φ contributions, leading to

$$-2\frac{P(\infty)}{C\theta} = \int dz \int dx (z^2 + x^2)^{-3} = \frac{\pi}{2a^4} \quad (15)$$

The difference ΔP between this value and that of P at finite R may be evaluated with an asymptotic expansion. We find

$$-8\frac{\Delta P}{C\theta} = \frac{3\pi}{8a^2} \quad (16)$$

so that the ratio

$$\frac{\Delta P}{P} = \frac{3}{16} \left(\frac{a}{R}\right)^2 \quad (17)$$

confirming the anticipated curvature dependence. A plausible near-neighbor cutoff is $a = (\pi/\theta)^{1/2} \sim 2 \text{ \AA}$. For a nanotube of $R_C = 7 \text{ \AA}$, the film is situated at $R \sim 4 \text{ \AA}$. Then the curvature correction to the energy per atom is about 5%.

TABLES

TABLE I. Properties of ^4He atoms in the axial and shell states at threshold for formation of the axial phase, as a function of radius R_C of the nanotube. The quantities r_{rms} , V_C , V_{tot} , r_{min} , μ_c , R , and E_0 are defined in the text.

R_C (Å)	6	7	8
r_{rms} (Å)	0.41	1.01	2.00
$-V_{tot}(r_{min})$ (K)	166	97	79
$-V_C(r_{min})$ (K)	60	40	33
r_{min} (Å)	0.00	1.25	2.41
θ_c (Å $^{-2}$)	0.113	0.114	0.117
$-\mu_c$ (K)	98	75	54
$-E_0$ (K)	197	180	170
R (Å)	3.06	4.07	5.07

TABLE II. Properties of ^3He atoms in the axial and shell states at threshold, as in Table I.

R_C (Å)	6	7	8
r_{rms} (Å)	0.56	1.03	1.96
$-V_{tot}(r_{min})$ (K)	155	95	77
$-V_C(r_{min})$ (K)	60	40	32
r_{min} (Å)	0.00	1.38	2.41
θ_c (Å $^{-2}$)	0.110	0.110	0.113
$-\mu_c$ (K)	88	72	51
R (Å)	3.04	4.05	5.02

TABLE III. Properties of H_2 molecules in the axial and shell states at threshold, as in Table I.

R_C (Å)	6	7	8
r_{rms} (Å)	—	0.55	1.38
$-V_{tot}(r_{min})$ (K)	54.0	437	311
$-V_C(r_{min})$ (K)	254	141	106
r_{min} (Å)	0.00	0.44	1.67
θ_c (Å $^{-2}$)	—	0.097	0.099
$-\mu_c$ (K)	—	385	261
$-E_0$ (K)	749	689	651
R (Å)	2.69	3.67	4.65

 TABLE IV. Properties of a ^3He - ^4He mixture in the axial and shell states at threshold, as in Table I.

R_C (Å)	6	7	8
r_{rms} (Å)	0.43	1.00	1.92
$-V_{tot}(r_{min})$ (K)	157	97	79
$-V_C(r_{min})$ (K)	60	32	19
r_{min} (Å)	0.00	1.36	2.35
$\theta_{3,c}$ (Å $^{-2}$)	0.110	0.109	0.112
$\theta_{4,c}$ (Å $^{-2}$)	0.114	0.114	0.117
$-\mu_c$ (K)	88	72	51

REFERENCES

- [1] T. W. Ebbesen, “Carbon nanotubes”, Physics Today, June 1996, p. 26; M. S. Dresselhaus and G. Dresselhaus, and P. C. Eklund, *Science of fullerenes and carbon nanotubes* (Academic Press, New York, 1997).
- [2] S. Inoue, N. Ichikuni, T. Suzuki, T. Uematsu, and K. Kaneko, J. Phys. Chem. B **102**, 4689 (1998); E. B. Mackie, R. A. Wolfson, L. M. Arnold, K. Lafdi, and A. D. Migone, Langmuir **13**, 7197 (1997); A. C. Dillon, K. M. Jones, T. A. Bekkedahl, C. H. Kiang, D. S. Bethune, and M. J. Heben, Nature **386**, 377 (1997).
- [3] C. T. White and J. W. Mintmire, Nature **394**, 29 (1998).
- [4] R. Radhakrishnan and K. E. Gubbins, Phys. Rev. Lett. **79**, 2847 (1997); M. Maddox, D. Ulberg, and K. E. Gubbins, Intl. J. Thermophysics **15**, 1115 (1994); S. Sokołowski and J. Fischer, Phys. Rev. A **41**, 6866 (1990).
- [5] M. W. Cole, M. Boninsegni, G. Stan, C. A. Ebner and V. H. Crespi, “Condensation of Helium in Nanotube Bundles” to be published in Phys. Rev. Lett.
- [6] W. A. Steele and M. J. Bojan, Adv. Coll. Interface Sci. **76-77**, 153 (1998); Y. F. Yin, Tim Mays, and Brian McEnaney, Langmuir 15, 8714 (1999)
- [7] G. Stan, S. M. Gatica, M. Boninsegni, S. Curtarolo, and M. W. Cole, Am. J. of Phys. **67**, 1170 (1999).
- [8] G. Stan, M. Boninsegni, V. H. Crespi, and M. W. Cole, J. Low Temp. Phys. **113**, 447 (1998).
- [9] A. M. Vidales, V. H. Crespi, and M. W. Cole, Phys. Rev. B **58**, R13426 (1998).
- [10] B. K. Peterson, K. E. Gubbins, G. S. Helfinger, U. M. B. Marconi, and F. Van Swol, J. Chem. Phys. **88**, 6487 (1988).
- [11] Q. Wang, S.R. Challa, D.S. Sholl, and J.K. Johnson, Phys. Rev. Lett. **82**, 956 (1999).
- [12] Q. Wang and J. K. Johnson, J. Phys. Chem. B **103**, 277 (1999) and J. Chem. Phys. **110**, 577 (1999); M. J. Bojan, and W. A. Steele, *Computer Simulations of Sorption in*

Model Cylindrical Pores, Proceedings, 5th Conference on Fundamentals of Adsorption, Asilomar, 1995, M. D. LeVan, Ed. (Kluwer, Amsterdam, 1996); M.J. Bojan, R. van Slooten, and W.A. Steele, *Computer Simulation Studies of the Storage of Methane in Microporous Carbons*, Separation Science and Technology **27**, 1837 (1992).

[13] G. Stan and M. W. Cole, *Surf. Sci.* **395**, 280 (1998) and *J. Low Temp. Phys.* **110**, 539 (1998).

[14] W. Teizer, R. B. Hallock, E. Dujardin, T. W. Ebbesen, *Phys. Rev. Lett.* **82**, 5305 (1999)

[15] A. Kuznetsova, J. T. Yates, Jr., J. Liu, and R. E. Smalley, "Physical adsorption of xenon in open single walled carbon nanotubes - observation of a quasi 1-D confined Xe phase", to appear in *J. Chem. Phys.*; S. Weber, S. Talapatra, C. Journet and A. D. Mignone, "Adsorption of Methane on Single-Wall Nanotubes" to appear in *Phys. Rev. B*.

[16] G. Stan, M. J. Bojan, S. Curtarolo, S. M. Gatica and M. W. Cole, "Uptake of gases in bundles of carbon nanotubes", submitted to *Phys. Rev. B*.

[17] An ideal gas regime at $T \equiv 0$ for He may or may not exist in a nanotube. Based on relevant points in the discussion below, we suspect that it does exist for ${}^4\text{He}$, but does not for ${}^3\text{He}$.

[18] L. W. Bruch, M. W. Cole, and E. Zaremba, *Physical Adsorption: Forces and Phenomena* (Oxford University Press, 1997).

[19] J. G. Dash, M. Schick, and O. E. Vilches, *Surf. Sci.* **299-300**, 405 (1994).

[20] This similarity of flat and curved films' energetics at $T=0$ contrasts with the thermal excitation behavior at low T. As discussed by Vidales *et al.*, Ref. [9], the curved film exhibits quasi-1d excitation in this regime.

[21] S. J. Gregg and K. S. W. Sing, *Adsorption, Surface Area and Porosity* (Academic Press, London, 1965).

[22] M. J. De Oliveira and R. B. Griffiths, *Surf. Sci.* **71**, 687 (1978).

- [23] Q. Wang and J. K. Johnson, unpublished.
- [24] P.A. Whitlock, G.V. Chester, and B. Krishnamachari, Phys. Rev. B **58**, 8704 (1998).
- [25] X.-Z. Ni and L. W. Bruch, Phys. Rev. B **33**, 4584 (1986).
- [26] R. L. Elgin and D. L. Goodstein, Phys. Rev. A **9**, 2657 (1974).
- [27] S. M. Gatica, E. S. Hernández, M. Barranco, J. Chem. Phys. **107**, 927 (1997); M. Barranco, Phys. Rev. B **49**, 12078 (1994).
- [28] E. Cheng, G. Ihm and M. W. Cole, J. L. Temp. Phys. **74**, 519 (1989).
- [29] See Ref. [8]; M. Boninsegni and S. Moroni, J. Low Temp. Phys. **118**, 1 (2000); M. E. Krotscheck and M. D. Miller, Phys. Rev. B. 60, 13028 and 13038 (1999); This negligible value of the 1d cohesive energy is to be contrasted to the non-negligible value of the 2d binding energy (~ 0.9 K), which plays a small role in determining the criterion for monolayer completion in Ref. [28], but is omitted from the analysis of Ref. [24]. For ${}^3\text{He}$, we expect $\epsilon_a = 0$, as in 2d. For H_2 , we estimate $|\epsilon_a| \leq 1$ K, which is negligible.
- [30] M. W. Cole, D. R. Frankl and D. L. Goodstein, Rev. Mod. Phys. **53**, 199 (1981).
- [31] M. Bretz, J. G. Dash, D. C. Hickernell, E. O. Mclean, and O. E. Vilches, Phys. Rev. A **8**, 1589 (1973).
- [32] The corresponding values for ${}^3\text{He}$ on graphite are 0.108 \AA^{-2} and -27 K; see Refs. [25,31].
- [33] M. Nielsen, J. P. McTague, and W. Ellenson, J. de Physique **38**, C4-10 (1977).
- [34] R.P. Feynman, Rev. Mod. Phys., **20**, 367 (1948); R.P. Feynman, and A.R.Hibbs, *Quantum Mechanics and Path Integrals* (McGraw-Hill, New York, 1965).
- [35] Q. Wang and J. K. Johnson, Mol. Phys., **95**, 299 (1998).
- [36] Q. Wang and J. K. Johnson, J. Chem. Phys., **110**, 577 (1999).
- [37] I.F. Silvera and V.V. Goldman, J. Chem. Phys., **69**, 4209 (1978).
- [38] M. D. Miller, Phys. Rev. B **17**, 1139 (1978); R. A. Guyer and M. D. Miller, Phys. Rev.

B **22**, 142 (1980).

- [39] J. M. Gottlieb and L. W. Bruch, private communication.
- [40] M. Boninsegni, M. W. Cole and F. Toigo, Phys. Rev. Lett. 83, 2002 (1999); F. Ancilotto, A. M. Sartori and F. Toigo, Phys. Rev. B 58, 5085 (1998).
- [41] F. Dalfovo, Z. Phys. D 29, 61 (1994); K. K. Lekmann, Mol. Phys, in press; G. De Toffol, F. Ancilotto, F. Toigo, J. Low. Temp. Phys. 102, 381 (1996).

FIGURES

FIG. 1. Upwards (downwards) sloping curves are the chemical potentials of the cylindrical (axial) phases for ^4He as a function of 2d shell density, θ_4 , in the cases of nanotubes with radii $R_C = 6, 7, 8 \text{ \AA}$, from bottom to top.

FIG. 2. Same as Fig. 1, but for ^3He .

FIG. 3. Hartree model calculations of probability density (unnormalized) for ^4He atoms in tubes of radius of 6 \AA (—), 7 \AA (— —) and 8 \AA (— · —).

FIG. 4. Curves are as in Fig. 1, except that no curve exists for $R_C = 6 \text{ \AA}$, as discussed in text.

FIG. 5. Hartree model calculations, discussed in text, of probability density for H_2 in tubes of radius $R_C = 6 \text{ \AA}$ (—), 7 \AA (— —) and 8 \AA (— · —). Note the absence of the axial phase for the case of a 6 \AA tube.

FIG. 6. Shell density (θ) and axial density (N_a/L) in a 7 \AA radius nanotube at a temperature of 10 K as computed by path integral grand canonical Monte Carlo.

FIG. 7. Shell density (θ) and axial density (N_a/L) in a 6 \AA radius nanotube at a temperature of 10 K as computed by path integral grand canonical Monte Carlo.

FIG. 8. Density profile in reduced units for hydrogen in a 6 \AA radius nanotube at 10 K. Note that the shell phase is progressively pushed outward as the axial phase is populated.

FIG. 9. Density profile in reduced units for hydrogen in a 7 \AA radius nanotube at 10 K.

FIG. 10. Shell density (θ) and axial density (N_a/L) in a 8 \AA radius nanotube at a temperature of 10 K as computed by path integral grand canonical Monte Carlo.

FIG. 11. Density profile in reduced units for hydrogen in a 8 \AA radius nanotube at 10 K.

FIG. 12. Equilibrium densities of the coexisting ^3He and ^4He phases.

FIG. 13. Schematic picture showing the separation of He isotopes and ^3He atoms (\circ) moving in the ^4He (\bullet) regions.

FIG. 14. The chemical potential of ^3He , μ_3 , as a function of coverage, θ_4 , in the case when the axial ^3He atoms go within the ^4He shell.

FIG. 15. Density profile of ^4He at $T = 0$ in the case of a nanotube of radius 6 Å from FRDF calculation.

FIG. 16. Axial phase total number density and shell density for ^4He in the 6 Å nanotube, from FRDF calculation.

FIG. 17. Energy per particle and chemical potential for ^4He in the 6 Å nanotube, from FRDF calculation. The dashed line shows the value of N/L at which the axial phase appears.

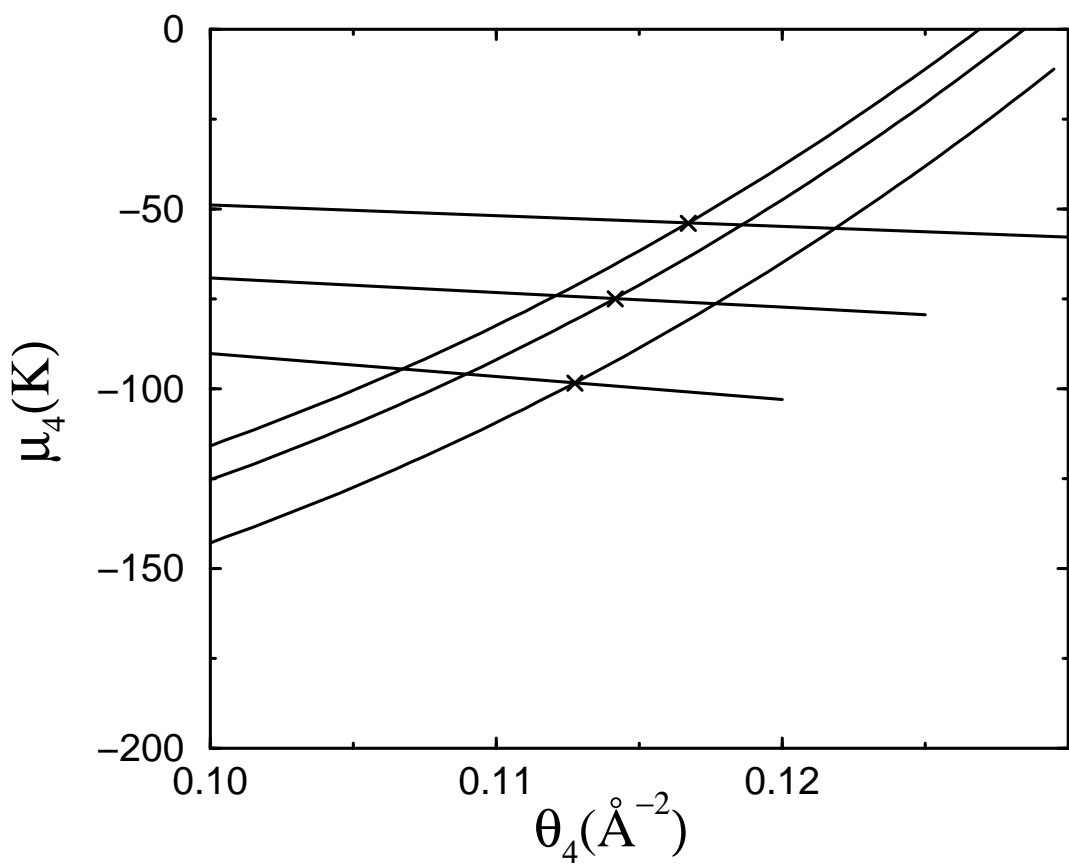


FIG. 1

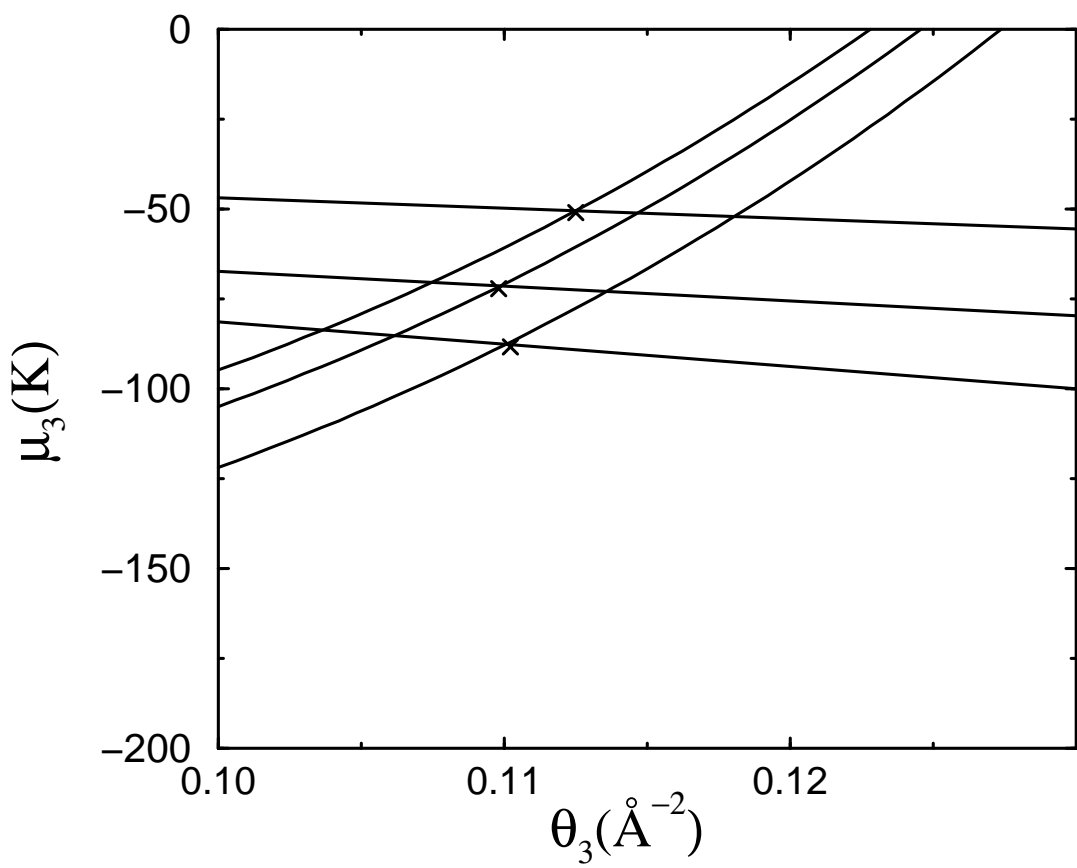


FIG. 2

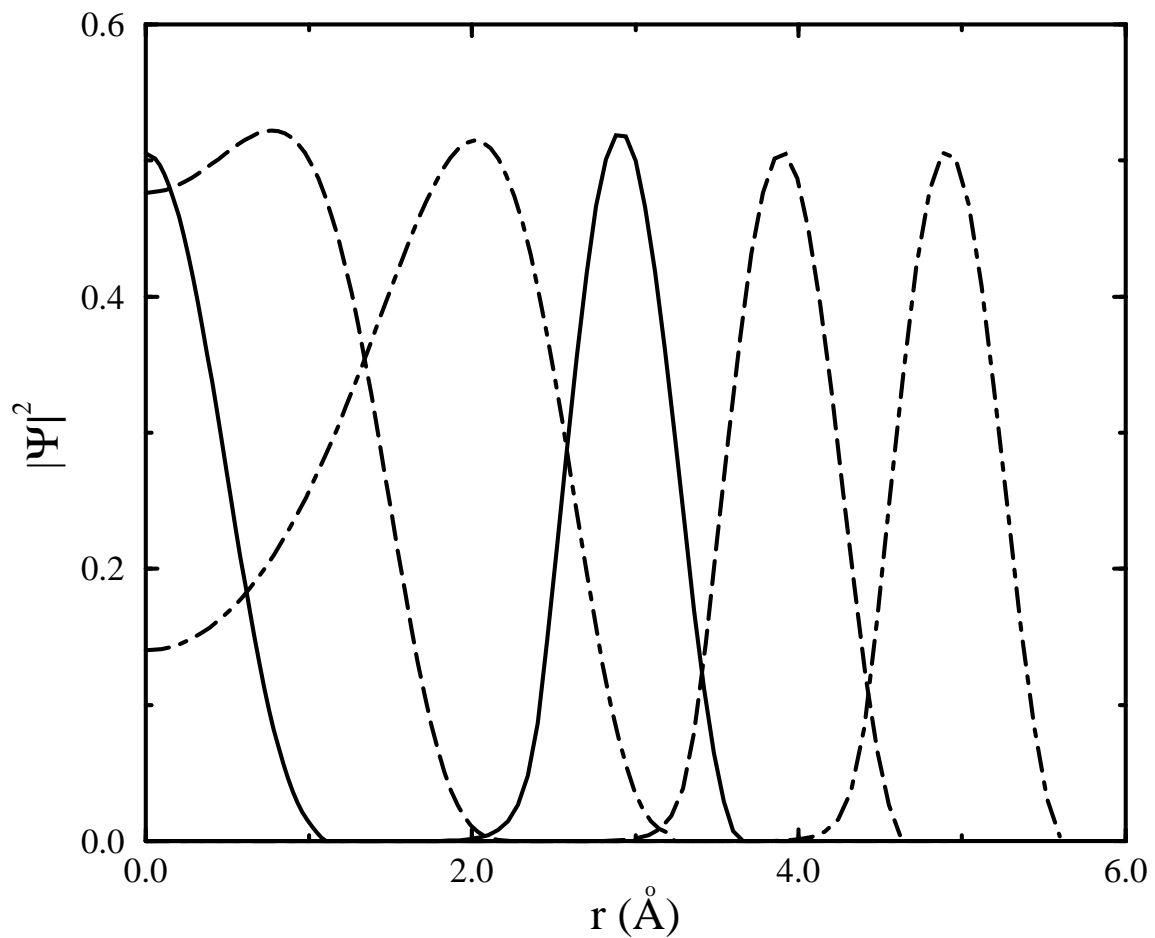


FIG. 3

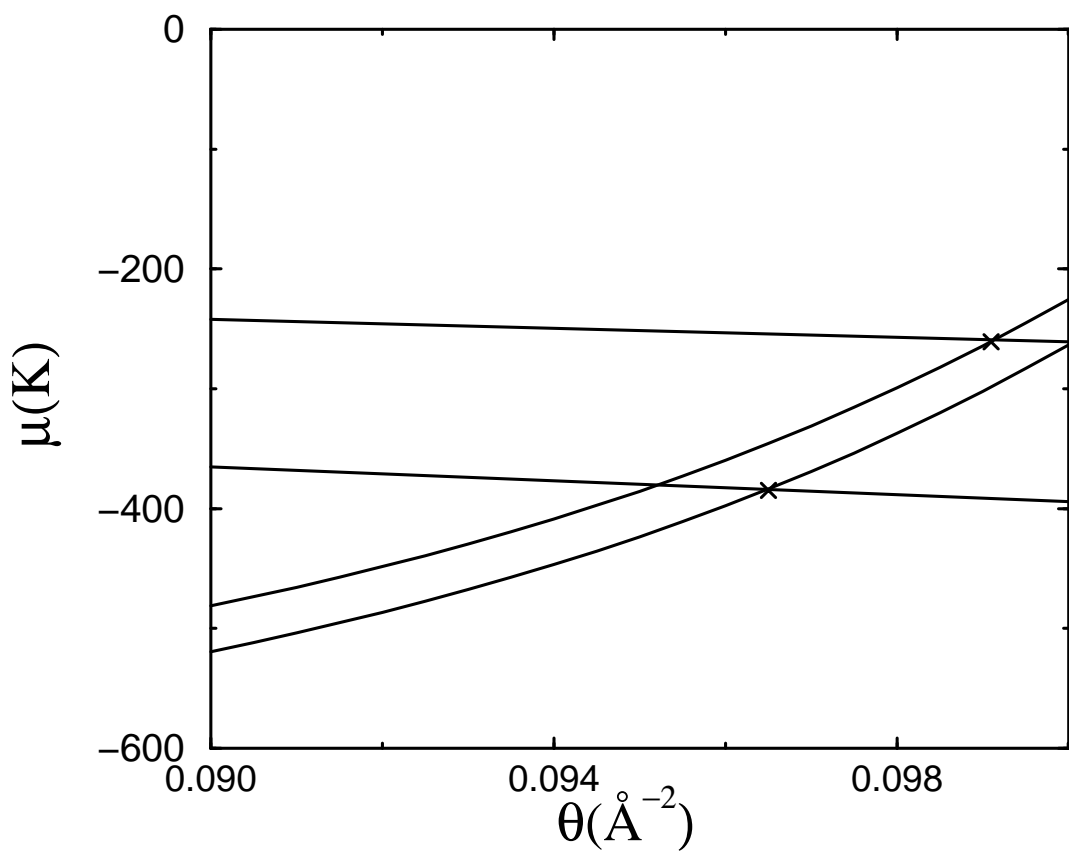


FIG. 4

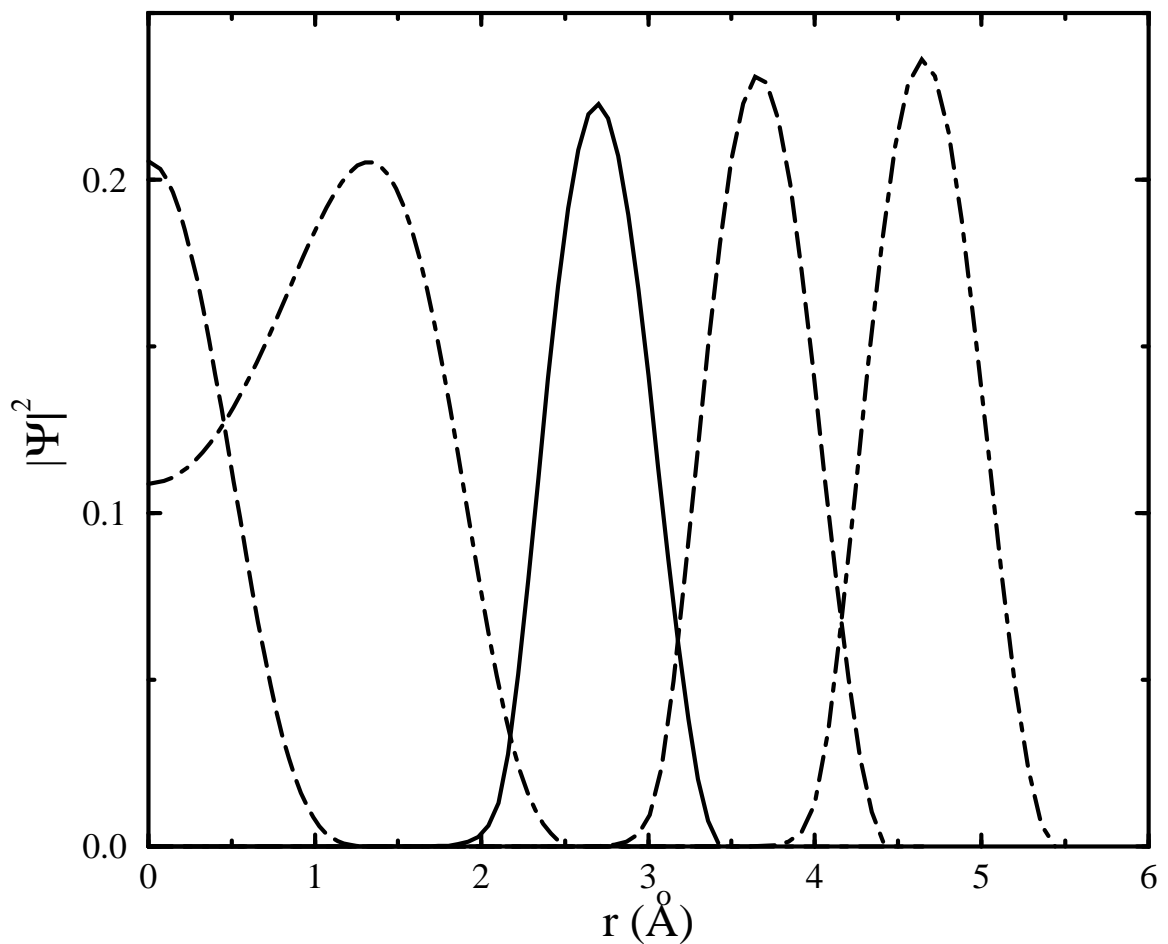


FIG. 5

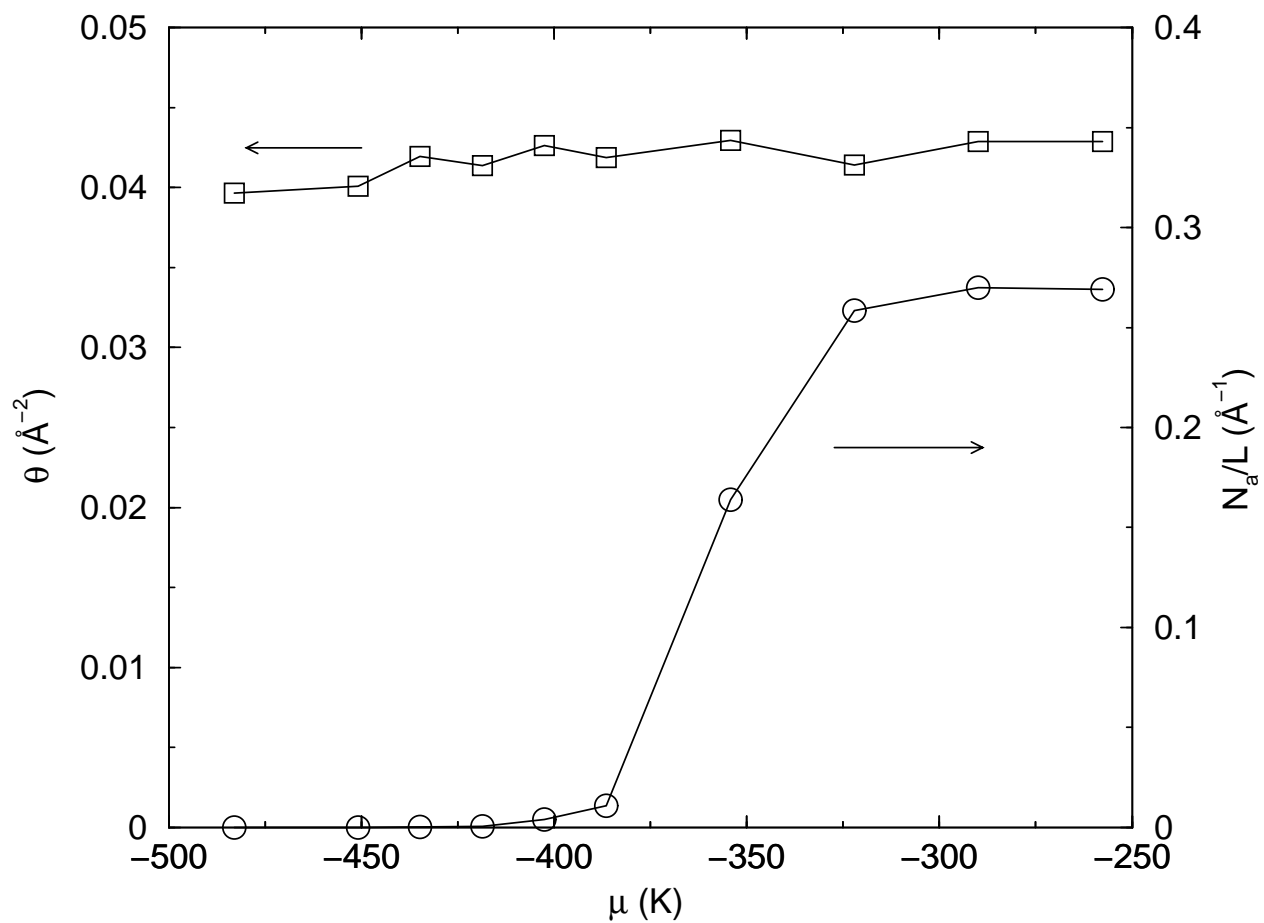


FIG. 6

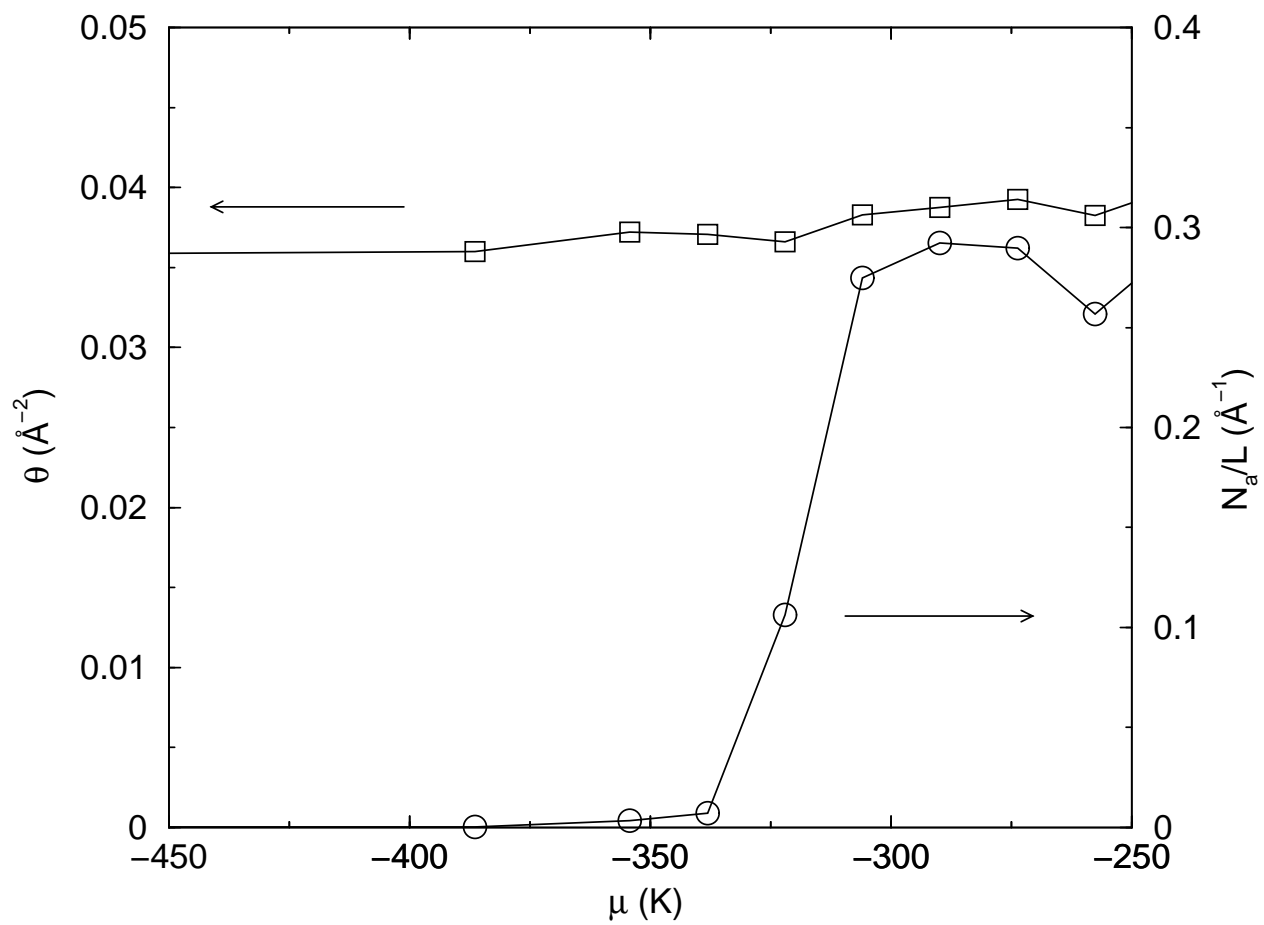


FIG. 7

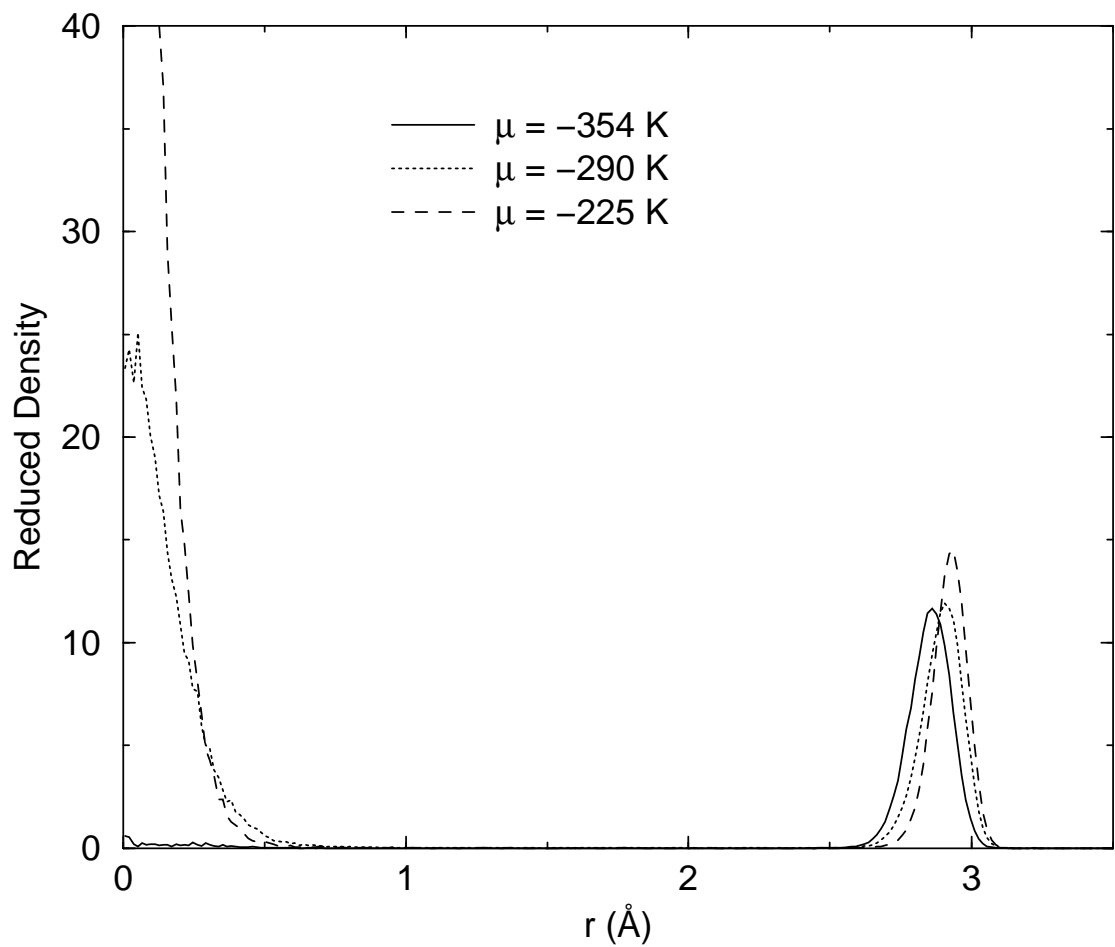


FIG. 8

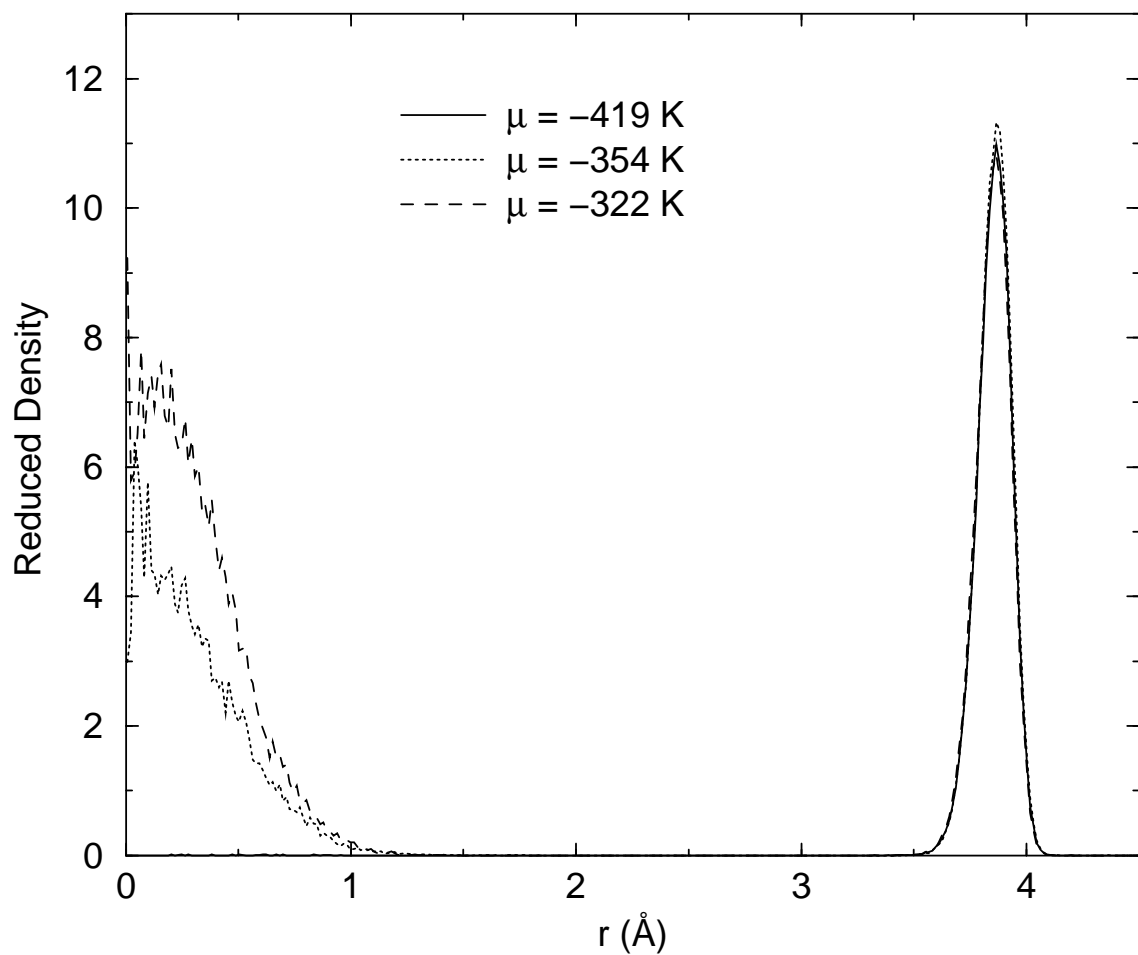


FIG. 9

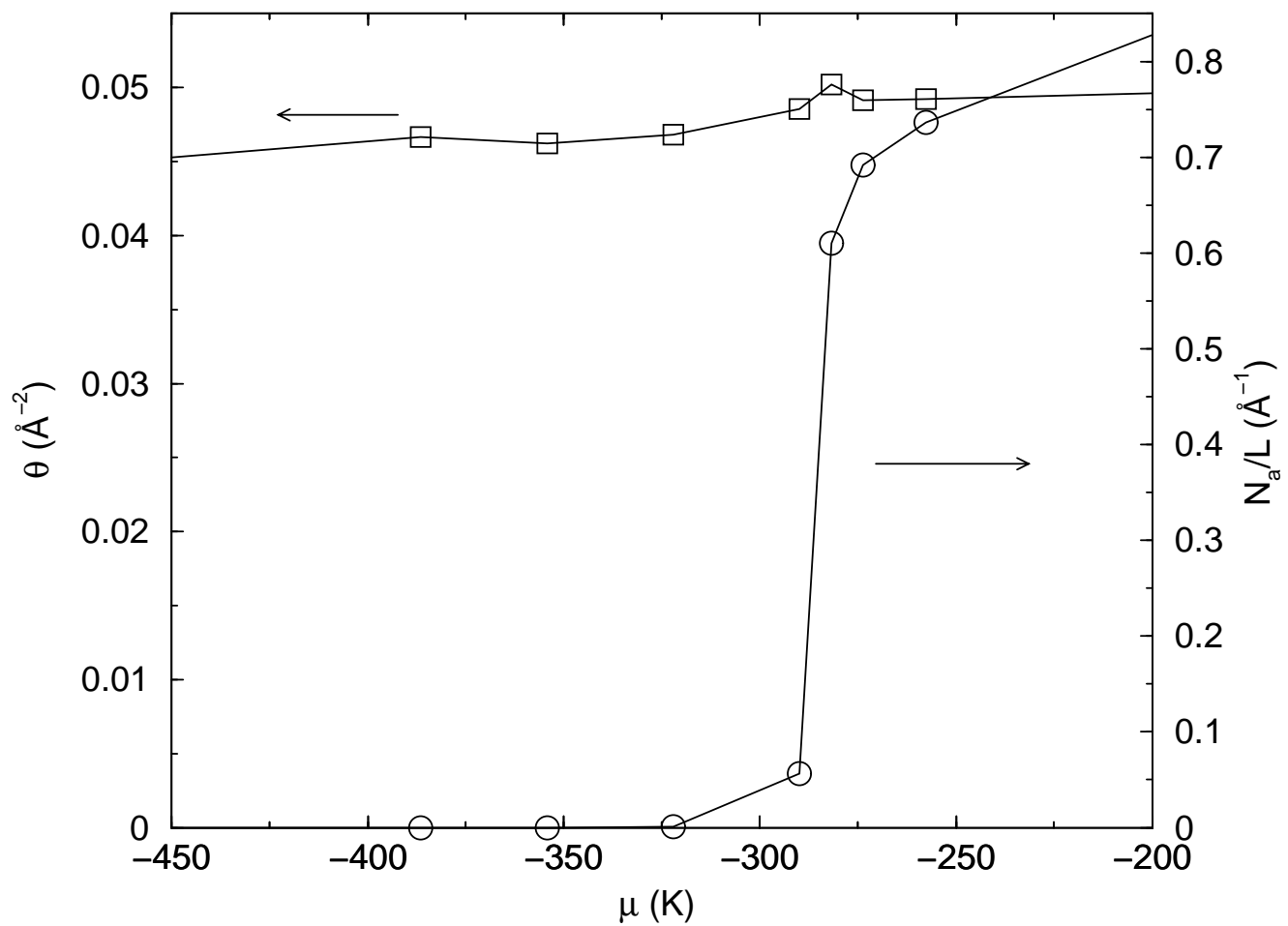


FIG. 10

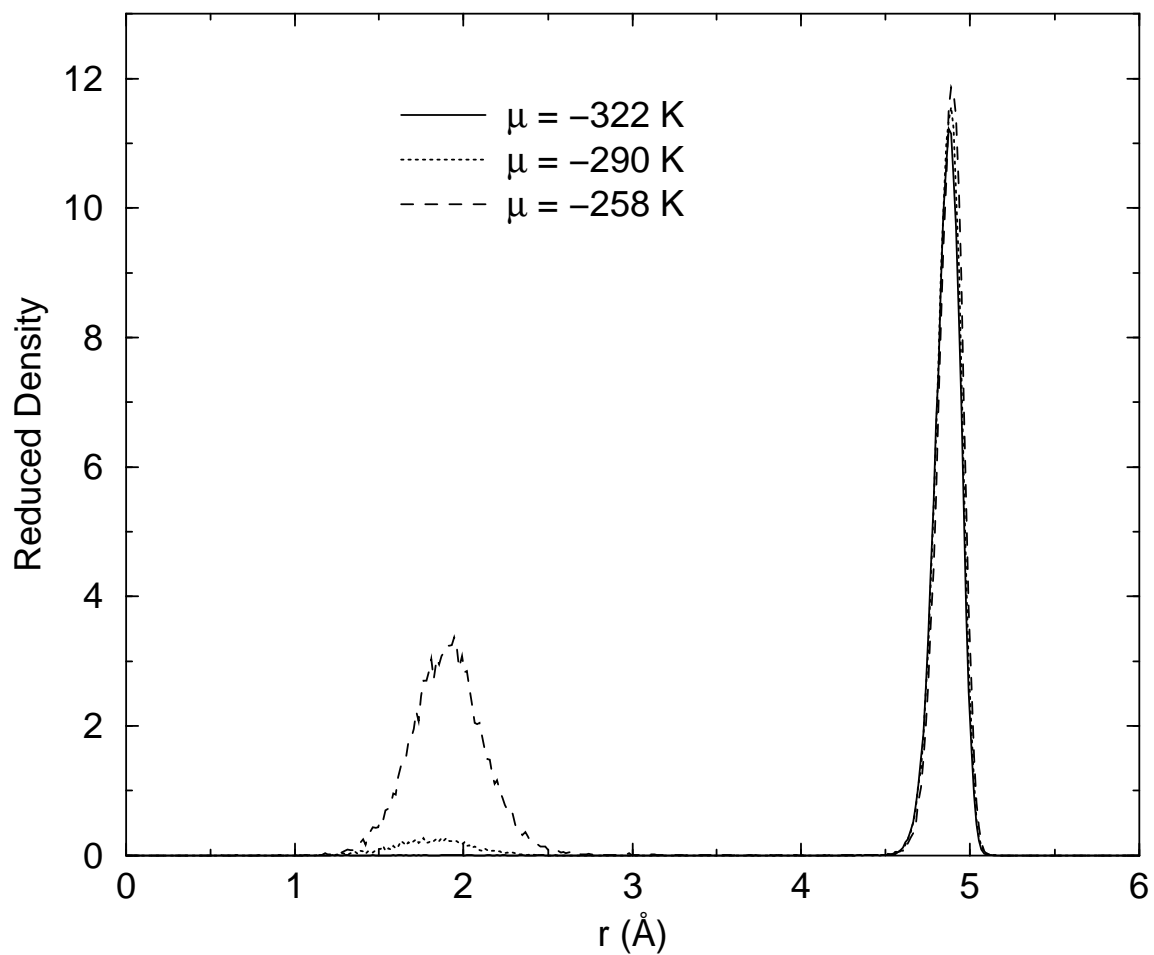


FIG. 11

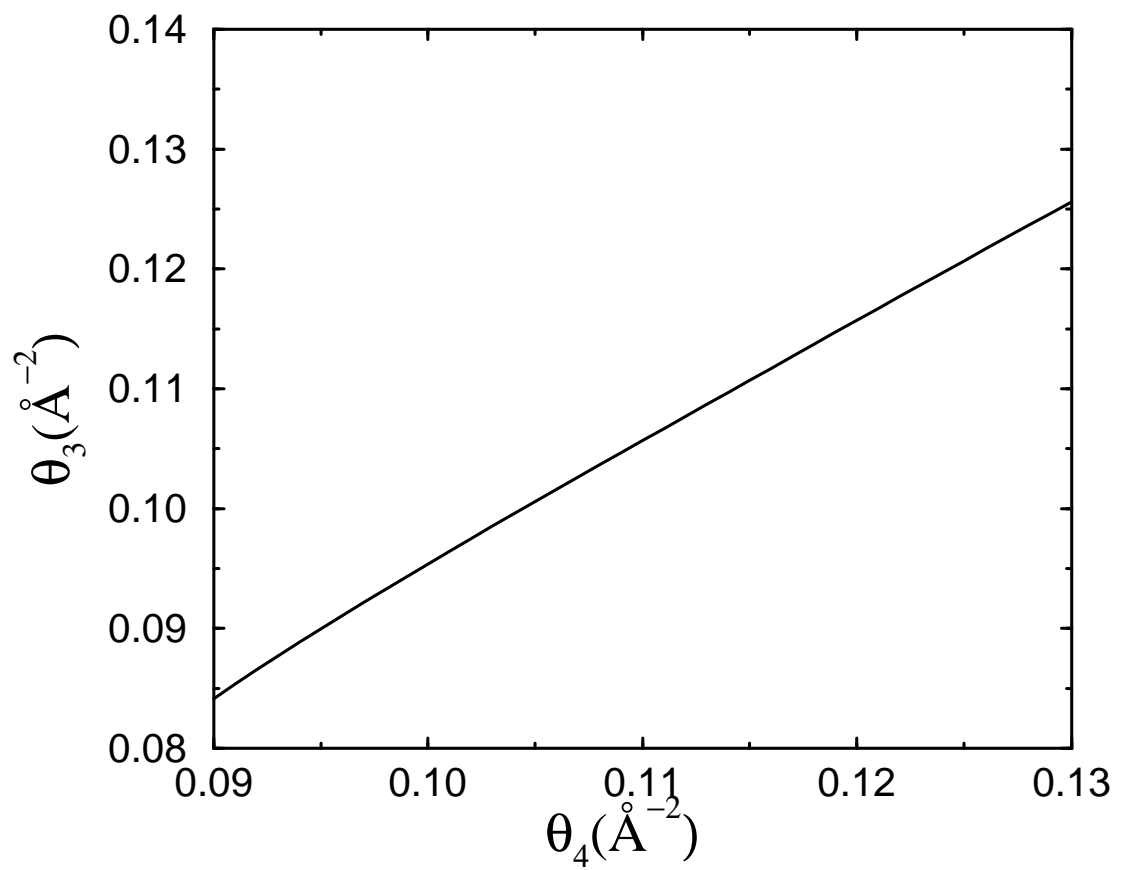


FIG. 12

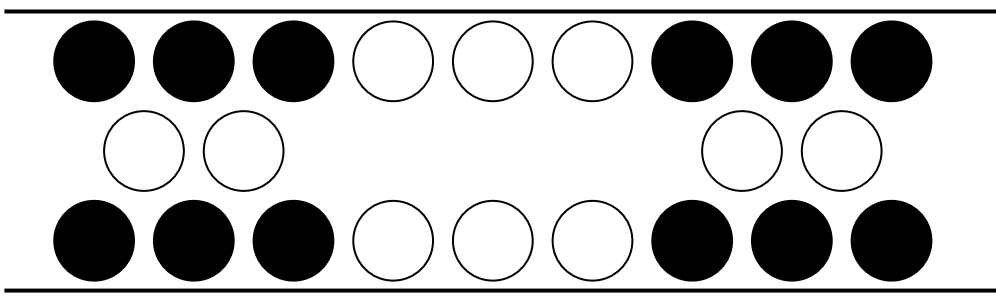


FIG. 13

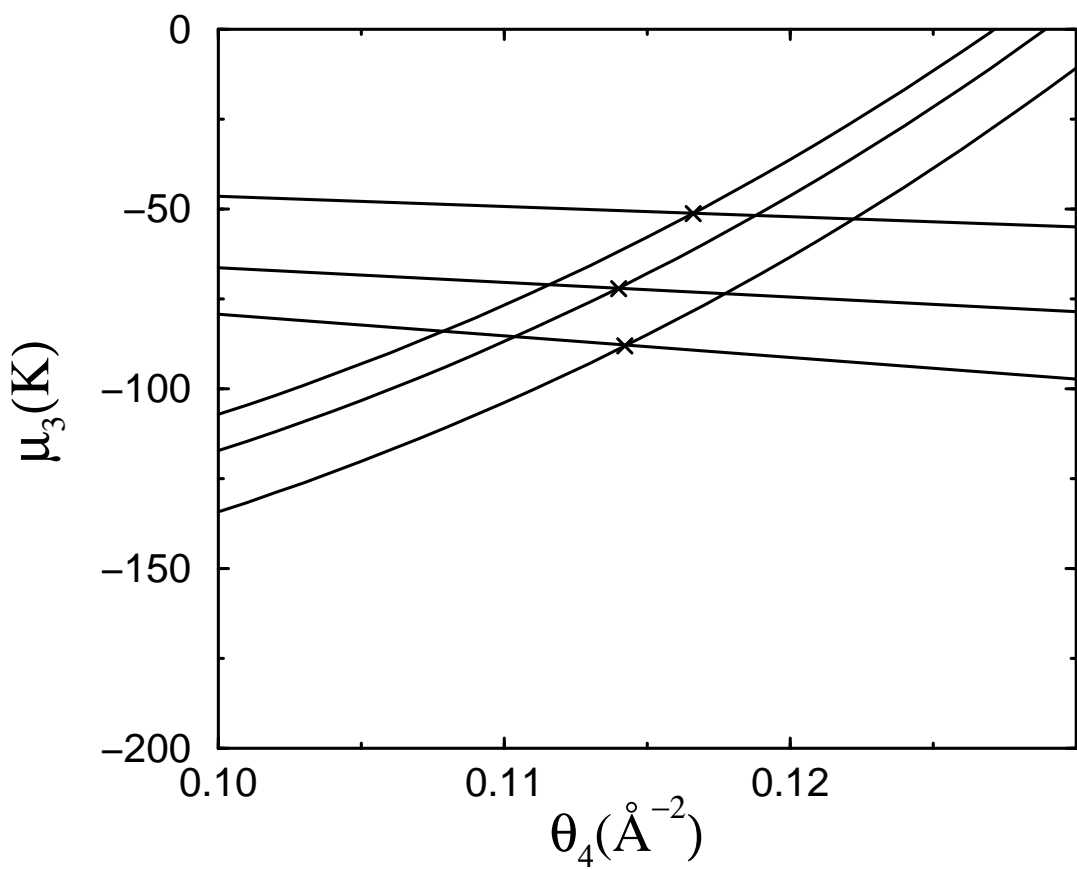


FIG. 14

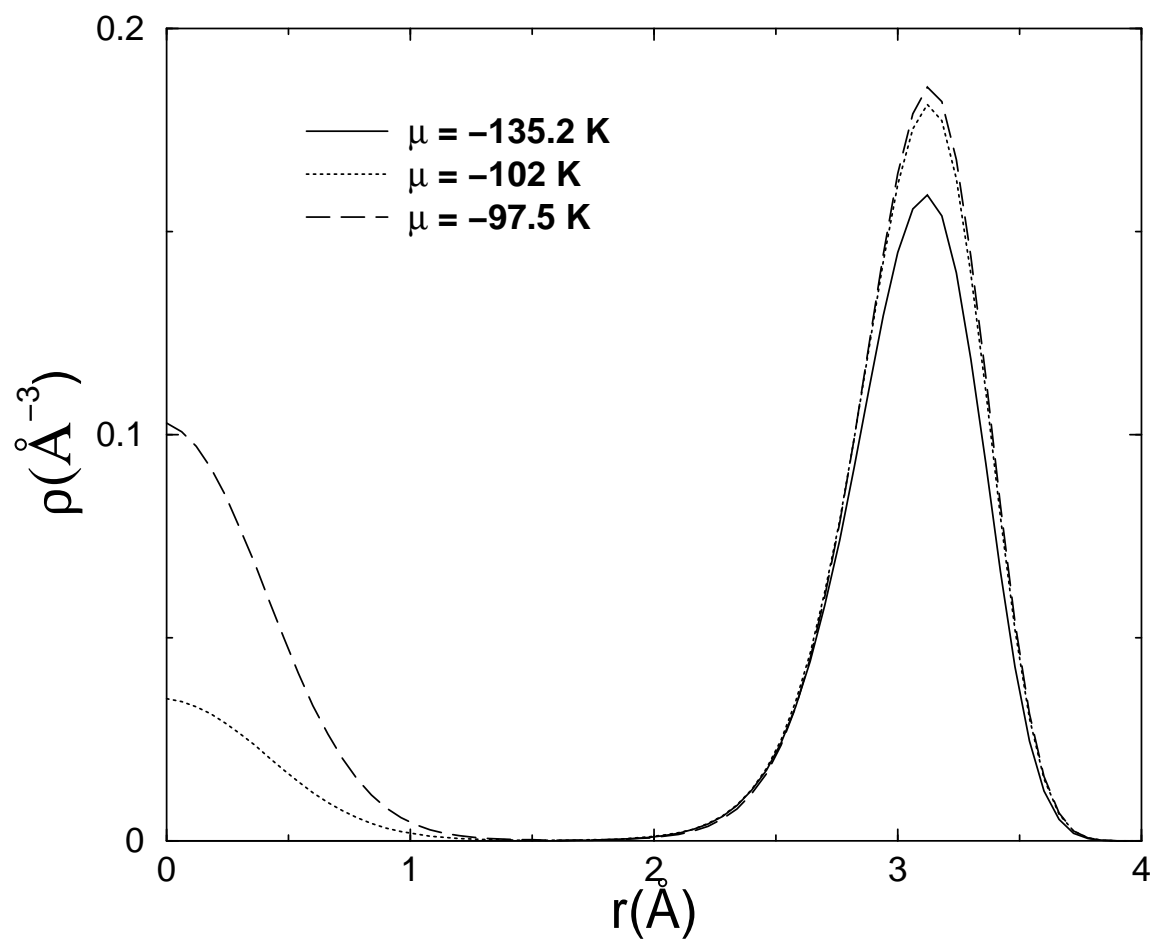


FIG. 15

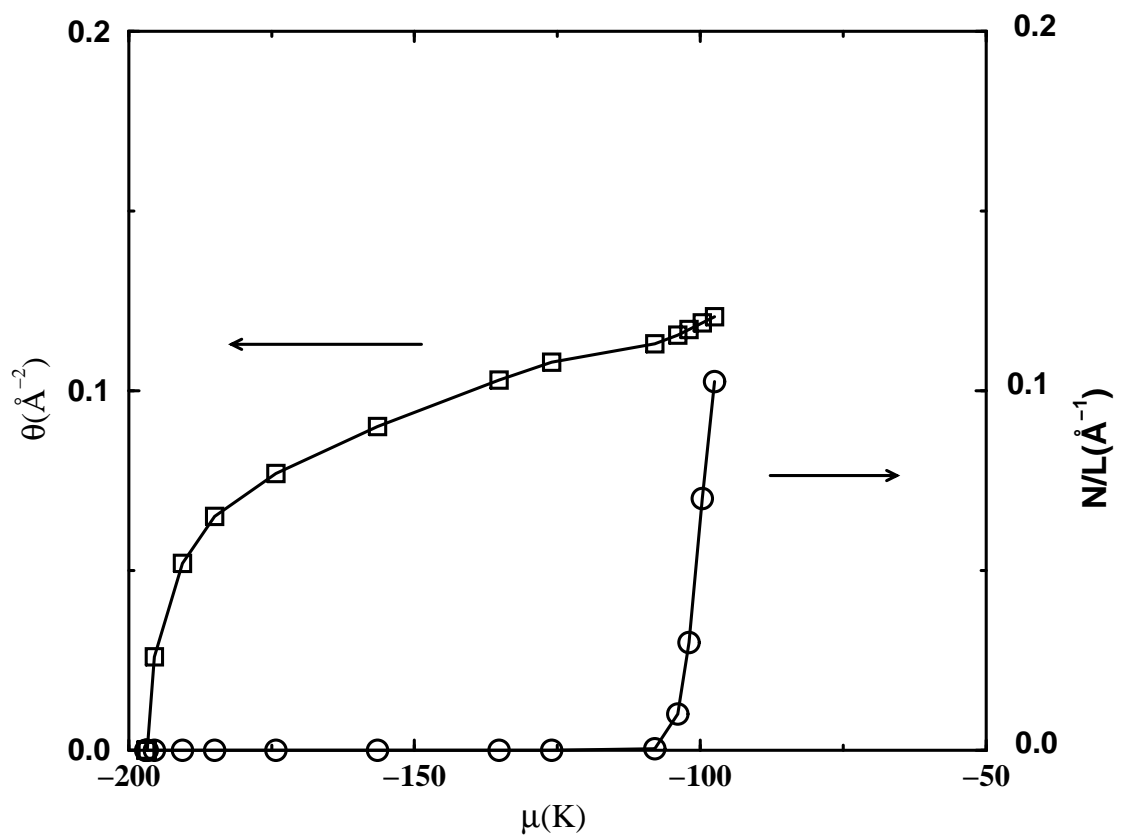


FIG. 16

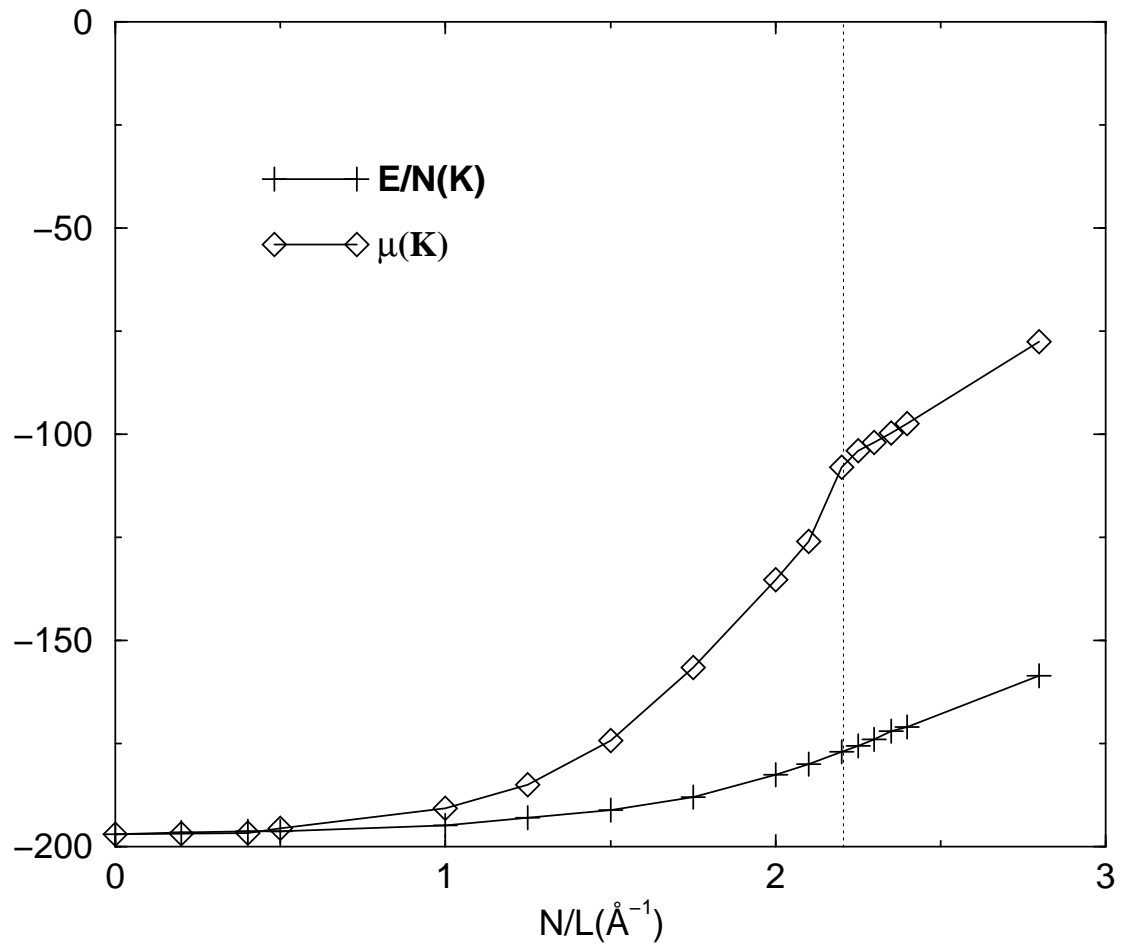


FIG. 17